Distorted Asymmetric Cubic Nanostructure of Soluble Fullerene Crystals in Efficient Polymer:Fullerene Solar Cells

Youngkyoo Kim,*,†,§ Jenny Nelson,*,† Tong Zhang,† Steffan Cook,‡ James R. Durrant,‡ Hwajeong Kim,⊥,§ Jiho Park,§ Minjung Shin,§ Sungho Nam,§ Martin Heeney,∥ Iain McCulloch,‡,∥ Chang-Sik Ha,# and Donal D. C. Bradley*,†

†Department of Physics, Blackett Laboratory, Imperial College London, Prince Consort Road, London SW7 2BW, United Kingdom, ‡Department of Chemistry, Imperial College London, Exhibition Road, London SW7 2AZ, United Kingdom, §Organic Nanoelectronics Laboratory, Department of Chemical Engineering, Kyungpook National University, Daegu 702-701, Republic of Korea, ⊥Institute of Biomedical Engineering, Imperial College London, Exhibition Road, London SW7 2AZ, United Kingdom, ∥Merck Chemicals, Chilworth Science Park, Southampton, United Kingdom, and #Department of Polymer Science and Engineering, Pusan National University, Pusan 609-735, Republic of Korea

ABSTRACT We found that 1-(3-methoxycarbonyl)propyl-1-phenyl-(6,6)C_{61} (PCBM) molecules make a *distorted* asymmetric body-centered cubic crystal nanostructure in the bulk heterojunction films of reigoregular poly(3-hexylthiophene) and PCBM. The wider angle of distortion in the PCBM nanocrystals was ~96°, which can be assigned to the influence of the attached side group to the fullerene ball of PCBM to bestow solubility. Atom concentration analysis showed that after thermal annealing the PCBM nanocrystals do preferentially distribute above the layer of P3HT nanocrystals inside devices.

KEYWORDS: polymer solar cells · soluble fullerene · asymmetric nanostructure · Raman scattering · field emission transmission electron microscopy

Finding ultrafast charge separation in conjugated polymer/fullerene blends has initiated keen interest in "bulk heterojunction (BHJ)" organic solar cells owing to their potential for cheap energy conversion device from solar light to electricity.[1−11] Although the power conversion efficiency has been improved up to ~6% via design of device structure and/or energy band engineering, the landmark work by Shaheen et al. is of crucial importance because it proved the importance of nanomorphology in the BHJ films for improving the device efficiency.[12−14] In addition, the reproducible 4−5% power conversion efficiency from the blend films of regioregular poly(3-hexylthiophene) (P3HT) and 1-(3-methoxycarbonyl)propyl-1-phenyl(6,6)C_{61} (PCBM) has paved a concrete base for the further improvement.[15−18] This achievement could be realized by optimizing blend (P3HT:PCBM) compositions, solvents, film thicknesses, and thermal annealing conditions. In particular, the thermal annealing did play a core role in enhancing the device efficiency because it drives the P3HT chains to crystallize leading to improved hole mobility and light absorption.[17,18]

In this regard, the nanostructure of P3HT in the blend films was widely studied using X-ray diffraction and transmission electron microscopy techniques.[17−21] However, a clear nanostructure of PCBM domains has not been observed in the optimized P3HT:PCBM films, even though some *d*-spacing values have been reported using electron diffraction patterns.[20−24]

In this work, we attempted to measure the nanostructure of PCBM domains in the P3HT:PCBM blend films for >4% efficiency polymer solar cells. As a result, we succeeded in measuring the images of PCBM nanocrystals embedded in the blend films and found that the PCBM nanocrystals were not aligned symmetrically but exhibited an asymmetric crystal structure.

RESULTS AND DISCUSSION

Although most previous studies showed that the efficiency of polymer solar cells made using P3HT:PCBM blend films was improved by thermal annealing,[15,17,18,25−28] the direct measurement of thermal transition temperature of the blend films was not yet studied in detail as a function of temperature though the film nanomorphology could be significantly influenced by the

*Address correspondence to ykimm@knu.ac.kr, y.kim@imperial.ac.uk.

Received for review May 13, 2009 and accepted August 19, 2009.

Published online September 1, 2009. 10.1021/nn900798m CCC: $40.75

© 2009 American Chemical Society

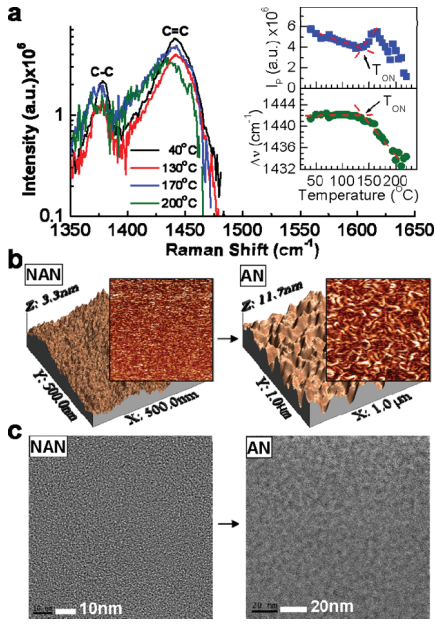

Figure 1. Spectroscopic and morphological change of P3HT:PCBM (1:1) blend film upon thermal annealing. (a) Raman back-scattering spectra of the blend film at selected annealing temperatures (excitation wavelength = 633 nm). Inset shows the detailed variation of Raman intensity (I_P) and spectral shift (ΔV) at the wavenumber of C═C stretching vibration as a function of temperature (T_{ON} denotes the onset temperature for a relaxation in the blend film). (b) 3D AFM images of the blend film before (left: NAN) and after (right: AN) thermal annealing at 140 °C for 2 h. The 2D images on the right top of each 3D image are the corresponding cosine-filtered images. (c) FE-TEM images of the blend film before (left: NAN) and after (right: AN) thermal annealing at 140 °C for 2 h.

chosen annealing temperature. Hence, first, we employed a Raman scattering technique to find the clear thermal annealing temperature range of the blend films.

As shown in Figure 1a, the as-coated (soft-baked) P3HT:PCBM (1:1 by weight) blend film exhibits two characteristic Raman vibrations at around 1380 and 1442 cm^{-1} which correspond to C−C skeletal and C═C stretching vibrations of thiophene rings, respectively[29] (we note that PCBM molecules also contribute to the Raman vibration at around 1442 cm^{-1}).[29,30] With increasing temperature, the peak position of the C═C stretching was maintained almost constant in the presence of slight oscillations, but a clear downward (to lower energy) shift was measured at 130−140 °C (see inset to Figure 1a). This indicates that the film morphology change was initiated at this temperature. In particular, the larger oscillation in the peak position at temperatures above 190 °C can be attributed to the further change of the film morphology as previously observed in the device characteristics.[31] Similarly, the peak intensity showed a critical change at 130−140 °C: The intensity increased up to 170 °C and then decreased, which might reflect the existence of intermediate states for local composition variation (vertically and/or horizontally inside film) during morphology change upon thermal annealing.[30] This result proves that the thermal transition of the P3HT:PCBM (1:1) blend film occurs at above 130 °C as the lowest but safely at 140 °C, which is in good agreement with previous results on device annealing.[15,17,18,26]

Hence, we tried to anneal devices at 130 and 140 °C for 2 h, but the results showed that the better performance was obtained for the 140 °C annealing.[18,28,31] We note that both 1:1 and 1:2 compositions showed similar effects by thermal annealing at this temperature (see Figure S1, Supporting Information). We focused, hereafter, mainly on the thermal annealing at 140 °C for 2 h. As shown in Figure 1b, thermal annealing under these conditions greatly changed the surface morphology of the blend film: The surface roughness of the annealed film was increased as much as more than three times [see the *Z*-axis value of atomic force microscopy (AFM) images]. In particular, from the cosine-filtered image we found semirigid coil-like nanowires with an average diameter of ∼10 nm or less, whereas no characteristic feature was observed from the as-coated film. In order to find further evidence on the morphology change upon thermal annealing, a high-resolution FE-TEM was employed. Similar to the AFM image, an almost no specially featured but very fine random crystal image was observed for the as-coated film (see Figure 1c). However, the FE-TEM image of the annealed film showed an "embossing" structure that seems to be closely related to the nanowires observed in the AFM image of the corresponding film (the shape of brighter whitish part in the FE-TEM image resembles that of the nanowires observed in the AFM image).

Hence, we attempted further increasing of the magnification and aperture-adjusting of the FE-TEM system and then found that the "embossing" parts of the annealed film in Figure 1c were not discrete nanowires but popped-up (to surface) assemblies of randomly ordered tiny crystals (see Figure 2a). That is, it is the coarse surface topology made during thermal annealing, as we noted the morphology change at this temperature from the Raman scattering results in Figure 1a. Compared to the FE-TEM image of pristine P3HT film (see Figure S2), these tiny crystals are considered to originate from P3HT molecules (chains). The longest length of these tiny crystals was ∼1 nm, while the crystal-to-crystal spacing (center-to-center) was ∼0.55 nm. Considering the chain length of P3HT polymer (refer to molecular weight), the crystal length seems to be too short so that the crystal images may not be originated from single crystals but from overlapping of several crystals in the direction normal to the film plane. We note that these tiny P3HT nanocrystal images were also found in the 1:2 composition, and the spacing was almost the same for both 1:1 and 1:2 composition after thermal annealing (see Figure S3). Thus, we can conclude that the examined region of the annealed blend film was a

P3HT-rich part, even though there must be some PCBM molecules that are not in a crystal form but in amorphous states (which cannot be detected by electron beam used for the FE-TEM measurement).

Here, the following question arises: *where are most of PCBM molecules are and how they can be found*? Are they molecularly dispersed in between the tiny P3HT crystal layers inside the film? This motivated us to perform a point-to-point examination on the annealed blend film. At low magnifications no special images were found, indicative of the absence of relatively huge nanoparticles or nanowires (see Figure S4). At some positions we found a very well aligned and ordered nanostructure whose size is approximately 20−30 nm wide (see Figure 2b). To date, this particular nanostructure has never been found in pristine P3HT films. Thus, we consider that this should be originated from PCBM molecules in the blend film. However, as shown in the enlarged image of Figure 2b, the size of each spot was much smaller than the diameter (0.71 nm) of C_{60}.[32−35] This means that these spots do not come from single PCBM molecules but from complex molecular arrangement, i.e., overlapping of PCBM molecules normal to the film plane: We note that if each single PCBM molecule shows a clear FE-TEM image, single PCBM molecules should be observed even in the as-coated (unannealed) blend film. In particular, the aligned lattice lines connecting each spot do not cross with a 90° angle but with ~96° for the wider angle (84° for the narrower angle) [also refer to the selected area electron diffraction (SAED) pattern in the inset of Figure 2b and Figure S5, Supporting Information]. In addition, the center-to-center distance of each spot was different: 0.36 nm in one direction and 0.44 nm in another direction (see the enlarged image in Figure 2b). However, the spot gaps are extremely regular in each direction over the measured area of ~20 nm or larger in the film. Thus, we conclude that only PCBM molecules can make this asymmetric molecular geometry owing to the attached side group [1-(3-methoxycarbonyl)propyl-1-phenyl group].[36] The wide-angle X-ray diffraction (WAXD) measurement resulted in the similar average *d*-spacing values of major peaks in the annealed pristine PCBM film (Figure S6, Supporting Information).

Based on the image in Figure 2b, we attempted to simulate possible arrangements of PCBM molecules, but only one structure could successfully match the measured image (see Figure 1c). We named this particular geometry a "distorted asymmetric body-centred cubic (*da-bcc*)" structure, considering the measured angle and spacing difference. The spots in the FE-TEM image are believed to originate from the close contact (stacked) geometry among top and bottom PCBM molecules which might intensify and/or strongly couple the electron density of each PCBM molecule so that they could be relatively well imaged (detected) in the FE-TEM measurement (see Figure S7, Supporting Information). Given the reported *d*-spacings of PCBM domains which are smaller than the diameter of fullerene ball,[20−23] we think that the present schematic illustration might be one of various spot images made by rotating the film axis. We note that the similar but slightly

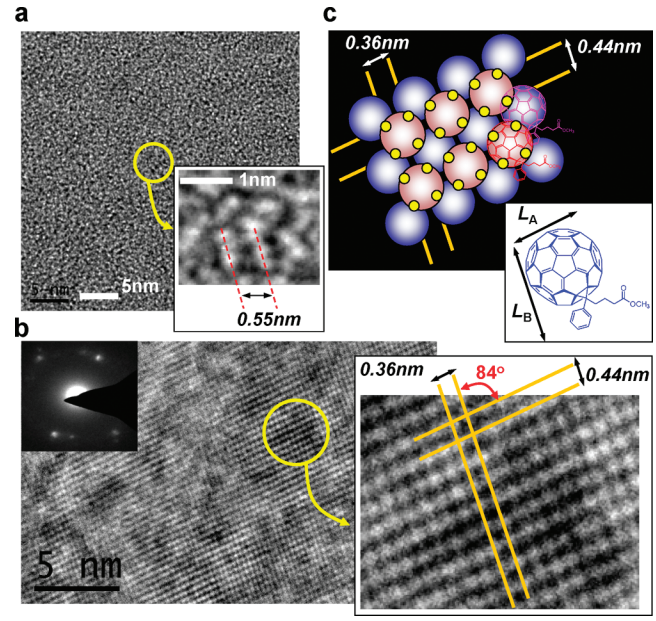

Figure 2. Aperture-adjusted and focused FE-TEM images of P3HT:PCBM (1:1) blend film annealed at 140 °C for 2 h: (a) FE-TEM image focusing on a P3HT-enriched region. (b) FE-TEM image focusing on a PCBM-enriched region (inset: part of SAED pattern). (c) Schematic illustration for the arrangement of PCBM molecules (the spheres represent the fullerene balls of PCBM) which leads to a distorted body-centered cubic (bcc) crystal structure: The apparent dimension of single PCBM molecule is marked with L_A (0.71 nm[32−35]) and L_B (~1.1 nm[36]) for the fullerene ball without and with the attached side group, respectively (left bottom figure).

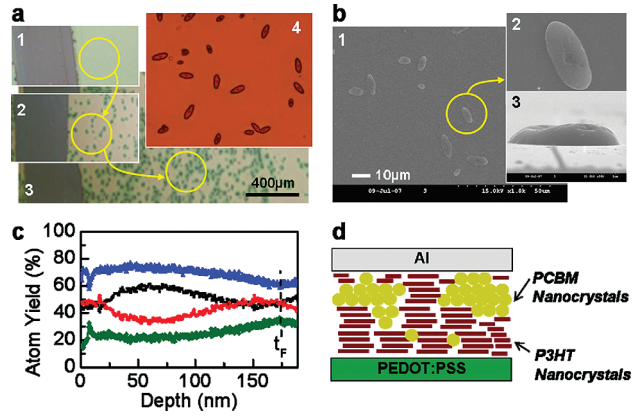

Figure 3. Semivertical alignment of molecules/nanocrystals in the P3HT:PCBM (1:1) blend film of devices. (a) Generation and growth of PCBM crystals to a micrometer size by extending annealing time: (1) 2 h, (2, 4) 5 h, and (3) 10 h. (b) FE-SEM images of PCBM microcrystals in the blend film (5 h annealing): (2) enlarged image focusing on the crystal in the image (1); (3) side view of the image (2). (c) GDS depth profiles of devices as a function of the blend film thickness: blue, green, black, and red colors represent carbon atoms in the not-annealed device, sulfur atoms in the not-annealed device, carbon atoms in the annealed device (140 °C/2 h), and sulfur atoms in the annealed device (140 °C/2 h), respectively. (d) Schematic illustration exhibiting a *semivertical* distribution of P3HT and PCBM nanocrystals in the optimized blend film (annealing time = 2 h).

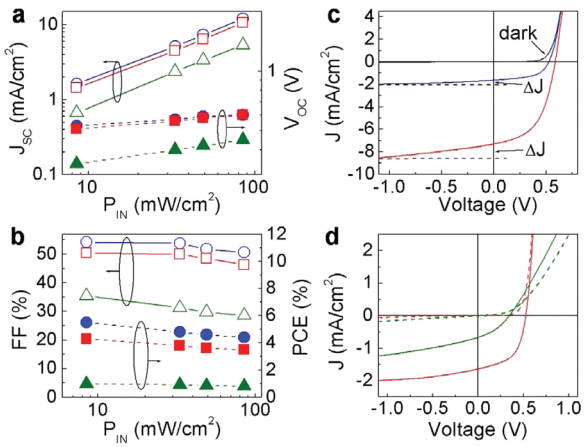

Figure 4. Device characteristics under AM1.5-simulated solar light illumination: (a, b) J_{SC}, V_{OC}, FF, and PCE as a function of P_{IN}: circles (annealed for 2 h), squares (annealed for 10 min), and triangles (not-annealed). (c) J−V characteristics of optimized (annealed for 2 h) device (blue curve: P_{IN} = 8.5 mW/cm^2, R_{SH} = 32.6 kΩ, R_S = 1.96 kΩ; red curve: P_{IN} = 48.9 mW/cm^2, R_{SH} = 13.0 kΩ, R_S = 0.54 kΩ). Note that the apparent slope of the dotted lines is the same as that of the dark $J-V$ curve at $V < 0$. (d) $J-V$ curves of optimized (annealed for 2 h) device (red dashed line under dark; red solid line at P_{IN} = 8.5 mW/cm^2) and not-annealed device (green dashed line under dark; green solid line at P_{IN} = 8.5 mW/cm^2, R_{SH} = 73.4 kΩ).

less ordered crystal feature was also found in the other position of the annealed blend film (see Figure S8, Supporting Information).

Since the above observations are all about the top view of the film, we still do not know about the vertical positioning of PCBM in the direction normal to the film plane, though we recently reported a related result obtained by optical measurement.[30] As shown in Figure 3a, further extending of annealing time resulted in the formation of microcrystals in the blend films which are considered to be overgrown PCBM particles: As the annealing time increased, the population of microcrystals increased but the size of microcrystals was irregular. As shown in Figure 3b, the field emission-scanning electron microscopy (FE-SEM) examination revealed that these microcrystals are enriched on the surface direction of the blend film: If they are likely to thermodynamically enrich to the substrate side, the top surface should be covered with P3HT skins.

Therefore, we can conclude that the PCBM nanocrystals tend to enrich toward the surface of the optimized blend film. Hence, the change of atom (molecule) concentration along with the thickness (t) direction of the blend film in devices was measured using glow discharge spectroscopy (GDS). As shown in Figure 3c, the relative distribution of P3HT (main indicator: sulfur atom) and PCBM (main indicator: carbon atom) molecules was considerably changed by thermal annealing. The PCBM composition after thermal annealing became slightly richer at the t = 30−100 nm position from the film surface, indicating a gradual formation of "*semivertical segregation*" p−n junction morphology (see Figure 3d) featuring PCBM molecules (n-type) and P3HT chains (p-type) that are richer close to the electron-collecting (Al) and hole-collecting (PEDOT:PSS/ITO) electrodes, respectively (see the energy band diagram in ref 26 for ideal p−n junction).[26]

Finally, we examined the characteristics of the optimized device that has a *da-bcc*-structured PCBM nanocrystals in the blend film. At high light intensity (85 mW/cm^2), the device performance was quite similar to that reported in ref 18 (PCE = ∼4.4%). However, at about half intensity (48.9 mW/cm^2), the PCE was slightly improved to ∼4.6% and then further enhanced to ∼5.5% at 10-fold lower intensity (8.5 mW/cm^2) (see Figure 4a,b). This light intensity-dependent PCE enhancement for the optimized device (annealed for 2 h) is apparently due to the improved fill factor (FF) and less reduced open circuit voltage (V_{OC}) for the optimized devices, compared to the less optimized devices. In particular, the shunt resistance (R_{SH}) was significantly improved from 7.5 kΩ (at 85 mW/cm^2) to 32.6 kΩ (at 8.5 mW/cm^2). This indicates that the degree of photoshunt was greatly reduced by lowering the light intensity, indicating the lowered charge recombination in the device (see different ΔJ for both cases in Figure 4c). We note that this improving effect was less pronounced for less optimized or unannealed device (see Figure 4b), which can be explained by their lower R_{SH} and higher series resistance (R_S) (see Figure 4d).

CONCLUSIONS

In summary, the outstanding characteristics of the optimized device can be attributed to (1) formation of *semivertically phase segregated* p−n junction morphology leading to greatly reduced charge recombination and charge blocking resistance (see R_{SH} and R_S)[37] and (2) generation of the *da-bcc* PCBM nanocrystal structure leading to the improved electron transport in devices.

EXPERIMENTAL SECTION

Materials. The same batch of regioregular P3HT (regioregularity = 95.4%) and PCBM described in refs 18 and 26 was used in this work. Blend solutions (P3HT:PCBM = 1:1 by weight) were prepared using chlorobenzene (CB) at a solid concentration of 50−60 mg/mL.

Fabrication of Films and Devices. P3HT:PCBM (1:1) blend films and solar cells were fabricated in the a similar way as in refs 18 and 26. The thickness of the blend films was ∼175 nm. Thermal annealing of films and devices was carried out inside a nitrogen-filled glovebox (oxygen and moisture level <1 ppm) at 140 °C with varying times up to 10 h.

Thermal Transition. The thermal transition of P3HT:PCBM blend films was measured using a reflection-mode Raman spectroscopy (Renishaw 2000 CCD spectrometer) equipped with a nitrogen-purged programmable hot stage (Linkam), in which the excitation wavelength was 633 nm from a He−Ne laser.

Surface Morphology. The surface nanomorphology of blend films was measured using a multimode scanning probe microscope system (tapping mode AFM, Digital Instrument, Inc.) in which a cosine-filtration process was carried out using the WSxM interactive software (Nanotec Electronica S. L., Spain) [see Horcas, I. et al. *Rev. Sci. Instrum.* **2007**, *78*, 013705].). The microcrystals on the surface of blend films were measured using a field emission-scanning electron microscope (FE-SEM, Hitachi).

Crystal Nanostructure. The crystal nanostructure of blend films was measured using FE-TEM (JEM-2100F, JEOL) equipped with a field emission gun (FEG, LaB_6 single crystal) at an electron acceleration voltage of 200 kV. For the preparation of TEM samples the blend films were lifted off from the substrate by dropping them into deionized water or vice versa, followed by mounting them on a 3 mm holey gold grid disk (300 mesh).

Vertical Distribution. The atom distribution along with the thickness direction of blend films was measured using a glow discharge spectrometer (GDS, JY10000RF, Jobin Yvon, France) equipped with a RF plasma (Ar ion) depth profiling system. The microcrystals on the surface of blend films were measured using a FE-SEM (Hitachi) and were double checked using an optical microscope (Karl Zeiss) with both transmission and reflection modes.

Device Characteristics. The photovoltaic characteristics of polymer solar cells were measured under an air mass (AM) 1.5 simulated solar light illumination using a solar simulator system (ScienceTech, Costronics Electronics) equipped with a Xe lamp and an AM 1.5 spectral filter. Calibration of the light intensity was achieved by using band-pass filters of known transmission combined with a silicon photodiode with independently certified spectral response, calibrated at the ISE-Fraunhofer Institute, Freiburg, Germany. The lamp intensity was adjusted to give close ($\pm$5%) agreement with theoretical one sun AM 1.5 intensity (P_{IN} = 100 mW/cm^2) over the spectral region of the optical absorption range (450−700 nm). Finally, the incident light intensity was recalibrated considering optical attenuation losses by sample holder windows, resulting in P_{IN} = 85 mW/cm^2. For the light intensity dependence experiment a set of neutral density filters was employed, and the resulting light intensity (P_{IN} = 8.5−85 mW/cm^2) was cross-checked using the calibrated silicon photodiode. In order to confirm the accuracy and reproducibility of measurements at low light intensity, we have compared the results with three methods: (1) normal measurement using the device that consists of six pixels, (2) each pixel of device was separated by scribing with a sharp scriber before measurement (we checked that no current flows between electrodes), and (3) only one pixel was exposed to the solar light whereas others were blocked with a black shadow mask. These three different methods showed almost similar device performance.

Acknowledgment. We thank Merck Chemicals Ltd. for supplying the P3HT polymer and BP Solar for financial support via the OSCER project. Y.K. thanks J. S. Kim and J. H. Choi of the Korea Basic Science Institute for help with FE-TEM measurements. This work was also financially supported by the Korean Government (Grant Nos. KOSEF-R01-2007-000-10836-0, KRF-2007-331-D00121, KETEP-2008-N-PV08-J-01-30202008, and KOSEF-20090072777).

Supporting Information Available: Detailed device performance for P3HT:PCBM = 1:1 and 1:2 compositions, UV−vis spectra, FE-TEM images, WAXD patterns, and schematic diagram. This material is available free of charge via the Internet at http://pubs.acs.org.

REFERENCES AND NOTES

1. Sariciftci, N. S.; Smilowitz, L.; Heeger, A. J.; Wudl, F. Photoinduced Electron Transfer from a Conducting Polymer to Buckminsterfullerene. *Science* **1992**, *258*, 1474–1476.
2. Halls, J. J. M.; Walsh, C. A.; Greenham, N. C.; Maeseglia, E. A.; Friend, R. H.; Moratti, S. C.; Holmes, A. B. Efficient Photodiodes from Interpenetrating Networks. *Nature* **1995**, *376*, 498–500.
3. Yu, G.; Gao, J.; Hummelen, J. C.; Wudl, F.; Heeger, A. J. Polymer Photovoltaic Cells: Enhanced Efficiencies via a Network of Internal Donor−Acceptor Heterojunctions. *Science* **1995**, *270*, 1789–1791.
4. Peumans, P.; Uchida, S.; Forrest, S. R. Efficient Bulk Heterojunction Photovoltaic Cells Using Small-Molecular-Weight Organic Thin Films. *Nature* **2003**, *425*, 158–162.
5. Günes, S.; Neugebauer, H.; Sariciftci, N. S. Conjugated Polymer-Based Organic Solar Cells. *Chem. Rev.* **2007**, *107*, 1324–1338.
6. Thompson, B. C.; Fréchet, J. M. J. Polymer-Fullerene Composite Solar Cells. *Angew. Chem., Int. Ed.* **2008**, *47*, 58–77.
7. Krebs, F. C. Fabrication and Processing of Polymer Solar Cells: A Review of Printing and Coating Techniques. *Sol. Energy Mater. Sol. Cells* **2009**, *93*, 394–412.
8. Krebs, F. C. Polymer Solar Cell Modules Prepared Using Roll-to-Roll Methods: Knife-over-Edge Coating, Slot-Die Coating and Screen Printing". *Sol. Energy Mater. Sol. Cells* **2009**, *93*, 465–475.
9. Dennler, G.; Scharber, M. C.; Brabec, C. J. Polymer-Fullerene Bulk-Heterojunction Solar Cells. *Adv. Mater.* **2009**, *21*, 1323–1338.
10. Krebs, F. C.; Gevorgyan, S. A.; Alstrup, J. A Roll-to-Roll Process to Flexible Polymer Solar Cells: Model Studies, Manufacture and Operational Stability Studies. *J. Mater. Chem.* **2009**, http://dx.doi.org/10.1039/B823001C.
11. Krebs, F. C. All Solution Roll-to-Roll Processed Polymer Solar Cells Free from Indium-Tin-Oxide and Vacuum Coating Steps. *Org. Electron.* **2009**, *10*, 761–768.
12. Kim, J. Y.; Lee, K.; Coates, N. E.; Moses, D.; Nguyen, T.; Dante, M.; Heeger, A. J. Efficient Tandem Polymer Solar Cells Fabricated by All-Solution Processing. *Science* **2007**, *317*, 222–225.
13. Park, S. H.; Roy, A.; Beaupré, S.; Cho, S.; Coates, N.; Moon, J. S.; Moses, D.; Leclerc, M.; Lee, K.; Heeger, A. J. Bulk Heterojunction Solar Cells with Internal Quantum Efficiency Approaching 100%. *Nature Photon.* **2009**, *3*, 297–302.
14. Shaheen, S. E.; Brabec, C. J.; Sariciftci, N. S.; Padinger, F.; Fromherz, T.; Hummelen, J. C. 2.5% Efficient Organic Plastic Solar Cells. *Appl. Phys. Lett.* **2001**, *78*, 841–843.
15. Reyes-Reyes, M.; Kim, K.; Dewald, J.; Sandoval, R.; Avadhanula, A.; Curran, S.; Carroll, D. L. Meso-structure Formation for Enhanced Organic Photovoltaic Cells. *Org. Lett.* **2005**, *7*, 5749–5752.
16. Li, G.; Shrotriya, V.; Huang, J.; Yao, Y.; Moriarty, T.; Emery, K.; Yang, Y. High-Efficiency Solution Processable Polymer Photovoltaic Cells by Self-Organization of Polymer Blends. *Nat. Mater.* **2005**, *4*, 864–868.
17. Ma, W.; Yang, C.; Gong, X.; Lee, K.; Heeger, A. J. Thermally Stable, Efficient Polymer Solar Cells with Nanoscale Control of the Interpenetrating Network Morphology. *Adv. Funct. Mater.* **2005**, *15*, 1617–1622.
18. Kim, Y.; Cook, S.; Tuladhar, S. M.; Choulis, S. A.; Nelson, J.; Durrant, J. R.; Bradley, D. D. C.; Giles, M.; McCulloch, I.; Ha, C. S.; Ree, M. A Strong Regioregularity Effect in Self-organizing Conjugated Polymer Films and High-efficiency Polythiophene:Fullerene Solar Cells. *Nat. Mater.* **2006**, *5*, 197–203.
19. Kim, Y.; Nelson, J.; Durrant, J. R.; Bradley, D. D. C.; Heo, K.; Park, J.; Kim, H.; McCulloch, I.; Martin, H.; Ree, M.; Ha, C. S. Polymer Chain/Nanocrystal Ordering in Thin Films of Regioregular Poly(3-hexylthiophene) and Blends with a Soluble Fullerene. *Soft Matter.* **2007**, *3*, 117–121.
20. Yang, X.; Loos, J.; Veenstra, S. C.; Verhees, W. J. H.; Wienk, M. M.; Kroon, J. M.; Michels, M. A. J.; Janssen, R. A. J. Nanoscale Morphology of High-performance Polymer Solar Cells. *Nano Lett.* **2005**, *5*, 579–583.
21. Reyes-Reyes, M.; Sandoval, R.; Arenas-Alatorre, J.; Garibay-Alonso, R.; Carroll, D. L.; Lastras-Martinez, A. Methanofullerene Elongated Nanostructure Formation for Enhanced Organic Solar Cells. *Thin Solid Films.* **2007**, *516*, 52–57.

22. Vanlaeke, P.; Swinnen, A.; Haeldermans, I.; Vanhoyland, G.; Aernouts, T.; Cheyns, Deibel, D. C.; D'Haen, J.; Heremans, P.; Poortmans, J.; Manca, J. V. P3HT/PCBM Bulk Heterojunction Solar Cells: Relation between Morphology and Electro-optical Characteristics. *Sol. Energ. Mater. Sol. Cell* **2006**, *90*, 2150–2158.
23. Swinnen, A.; Haeldermans, I.; Vande Ven, M.; D'Haen, J.; Vanhoyland, G.; Aresu, S.; D'Olieslaeger, M.; Manca, J. Tuning the Dimensions of C_{60}-based Needlike Crystals in Blended Thin Films. *Adv. Funct. Mater.* **2006**, *16*, 760–765.
24. Bavel, S. S.; Sourty, E.; de With, G.; Loos, J. Three-Dimensional Nanoscale Organization of Bulk Heterojunction Polymer Solar Cells. *Nano Lett.* **2009**, *9*, 507–513.
25. Padinger, F.; Ritterberger, R. S.; Sariciftci, N. S. Effects of Postproduction Treatment on Plastic Solar Cells. *Adv. Funct. Mater.* **2003**, *13*, 85–88.
26. Kim, Y.; Choulis, S. A.; Nelson, J.; Bradley, D. D. C.; Cook, S.; Durrant, J. R. Device Annealing Effect in Organic Solar Cells with Blends of Regioregular Poly(3-hexylthiophene) and Soluble Fullerene. *Appl. Phys. Lett.* **2005**, *86*, 063502.
27. Brabec, C. J. Organic Photovoltaics: Technology and Market. *Sol. Energ. Mater. Sol. Cell.* **2004**, *83*, 273–292.
28. Kim, J. Y.; Kim, S. H.; Lee, H.-H.; Lee, K.; Ma, W.; Gong, X.; Heeger, A. J. New Architecture for High-efficiency Polymer Photovoltaic Cells using Solution-based Titanium Oxide as an Optical Spacer. *Adv. Mater.* **2006**, *18*, 572–576.
29. Klimov, E.; Li, W.; Hoffmann, G. G.; Loos, J. Scanning Near-field and Confocal Raman Microscopic Investigation of P3HT-PCBM Systems for Solar Cell Applications. *Macromolecules* **2006**, *39*, 4493–4496.
30. Compoy-Quiles, M.; Ferenczi, T.; Agostinelli, T.; Etchegoin, P. G.; Kim, Y.; Anthopoulous, T.; Stavrinou, P. N.; Bradley, D. D. C.; Nelson, J. Morphology Evolution via Self-organisation and Lateral and Vertical Diffusion in Polymer: Fullerene Solar Cell Blends. *Nat. Mater.* **2008**, *7*, 158–164.
31. Kim, Y.; Choulis, S. A.; Nelson, J.; Bradley, D. D. C.; Cook, S.; Durrant, J. R. Composition and Annealing Effects in Polythiophene/Fullerene Solar Cells. *J. Mater. Sci.* **2005**, *40*, 1371–1376.
32. Kroto, H. W.; Heath, J. R.; O'Brien, S. C.; Curl, R. F.; Smalley, R. E. C_{60}: Buckminsterfullerene. *Nature* **1985**, *318*, 162–163.
33. Curl, R. F.; Smalley, R. E. Probing C_{60}. *Science* **1988**, *242*, 1017–1022.
34. Kroto, H. W. Space, Stars, C_{60}, and Soot. *Science* **1988**, *242*, 1139–1145.
35. Heiney, P. A.; Fischer, J. E.; McGhie, A. R.; Romanow, W. J.; Denenstein, A. M.; McCauley, J. P.; Smith, A. B. Orientational Ordering Transition in Solid C_{60}. *Phys. Rev. Lett.* **1991**, *66*, 2911–2914.
36. The size of L_B (~1.1 nm) was roughly calculated using the average C−C/C═C bond length of ~0.12 nm.
37. Kim, Y.; Cook, S.; Choulis, S. A.; Nelson, J.; Durrant, J. R.; Bradley, D. D. C. Organic Photovoltaic Devices Based on Blends of Regioregular Poly(3-hexylthiophene) and Poly(9,9-dioctylfluorene-co-benzothiadiazole). *Chem. Mater.* **2004**, *16*, 4812–4818.